Turkish Journal of Physics

http://journals.tubitak.gov.tr/physics/

Research Article

Turk J Phys
(2019) 43: 442 – 458
© TÜBİTAK
doi:10.3906/fiz-1903-15

Pseudoscalar Higgs boson pair production at a photon–photon collision in the two Higgs doublet model

Mehmet DEMİRCİ*
Department of Physics, Faculty of Science, Karadeniz Technical University, Trabzon, Turkey

Received: 19.03.2019 • **Accepted/Published Online:** 20.07.2019 • **Final Version:** 21.10.2019

Abstract: In this study, the direct pair production of the pseudoscalar Higgs boson at a $\gamma\gamma$ collision is analyzed in the context of the two Higgs doublet model (THDM), taking into account the complete one-loop contributions. In order to illustrate the effect of the new physics, four benchmark point scenarios, which are consistent with theoretical and current experimental constraints, are chosen in the type-I THDM with an exact alignment limit. The effect of individual contributions from each type of one-loop diagram on the total cross-section is examined in detail. The dependence of the cross-section on the center-of-mass energy is also presented at the various polarization configurations of the incoming photons. Moreover, the regions $m_{12}^2 - \tan\beta$ and $m_A - \tan\beta$ in the parameter space of the THDM are scanned for some fixed values of other parameters. The box-type diagrams make a much bigger contribution to the cross-section than the others at high energies. The total cross-section can be enhanced by a factor of two thanks to opposite-polarized photons as well as threshold effects.

Key words: Two Higgs doublet model, pseudoscalar Higgs boson, photon–photon collider, future electron–positron colliders

1. Introduction

The properties of a resonance at about 125 GeV[1] discovered at the Large Hadron Collider (LHC) [1, 2], consistent so far with the Higgs boson of the Standard Model (SM), confirms its particle content [3]. However, there are still mysteries here. The Higgs couplings are not universal, as the gauge couplings are, and their pattern is not explained by the SM. This discovery has triggered the search for new scalars as predicted by beyond SM (BSM) models with extended Higgs sectors. One of the simplest such extensions is the two Higgs doublet model (THDM) [4], which includes one extra Higgs doublet compared to the SM. Versions of the THDM emerge in various well-motivated scenarios for new BSM physics, with or without SUSY [5], where the extra Higgs doublet is either a necessary component or an essential byproduct in addressing problems such as the gauge hierarchy problem, the origin of dark matter, the strong CP problem, and the generation of baryon asymmetry. Additionally, given the multiplicity of Higgs states in the THDM, its scalar potential is significantly more involved than that of the SM. The THDM has a multitude of triple self-couplings, unlike the SM, which only

*Correspondence: mehmetdemirci@ktu.edu.tr

[1]The combined mass measurement (obtained from the data at $\sqrt{s} = 7$ and 8 TeV by the ATLAS&CMS experiments) is $m_h = 125.09 \pm 0.21(\text{stat.}) \pm 0.11(\text{syst.})$ GeV.

This work is licensed under a Creative Commons Attribution 4.0 International License.

has one. The triple and quartic couplings of Higgs bosons are key to understanding the phenomenology of the THDM, because they identify the form of the potential. To test the nature of Higgs bosons, the measurement of such couplings will be particularly important. Measurements at the LHC are rather challenging, due to requiring huge luminosity. In this context, future linear colliders would play an important role. Thanks to the clean environment, these couplings can be precisely identified as model-independent by these colliders. One of the most improved plans for a future linear collider is the International Linear Collider (ILC) [6, 7], which is designed to give facilities for e^-e^+ along with other options such as e^-e^-, $e^-\gamma$, and $\gamma\gamma$. Furthermore, there is an organization that brings ILC and Compact Linear Collider (CLIC) [8] projects together under one roof, which is called the Linear Collider Collaboration (LCC) [9]. The primary tasks of the LCC will be to extend and complement the results obtained at the LHC and to search for new BSM physics. The $\gamma\gamma$-colliders are also considered as the next option with about 100 fb^{-1} annual integrated luminosity. The machine is expected to be upgradeable to the range of $\sqrt{s} = 1000$ GeV with a total annual integrated luminosity up to 300 fb^{-1} [10]. Besides the possibility of discovering relatives of the Higgs boson by studying the properties of the 125 GeV Higgs boson, the ILC provides excellent opportunities to discover additional lighter Higgs bosons or, more generally, any weakly interacting light scalar or pseudoscalar particle by their direct production [11].

The main mechanism of production of pseudoscalar Higgs bosons at a $\gamma\gamma$ collider is $\gamma\gamma \to A^0$ [12–14]. However, in order to research the relevant quartic and triple couplings at future linear colliders, the pair production mode needs to be studied. The $\gamma\gamma$-colliders may supply a distinct method for pair production of the pseudoscalar Higgs boson. Furthermore, the production of neutral particle pairs in photon–photon collisions could be significantly sensitive to NP effects as such a process is naturally subdued. Consequently, an exhaustive test can be provided for the construction of extended Higgs sectors. The triple Higgs couplings in the THDM have been widely examined at electron–positron colliders [15, 16] and were found to supply an opportunity for the measurement of those couplings. The pair production of pseudoscalar Higgs bosons at $\gamma\gamma$ colliders in the Minimal Supersymmetric Standard Model has been extensively studied; however, there are few works on the THDM. The cross-sections for the fusion processes $\gamma\gamma \to S_iS_j$ $(S_i = h^0, H^0, A^0)$ were computed in [17] and a wide parameter region was shown where the cross-sections are larger by two orders of magnitude as compared to those of the SM. In the context of the type-III THDM, the pair production of the neutral Higgs boson at a $\gamma\gamma$ collider was also studied in [18]. Those authors pointed out that the relevant processes are significantly dependent on the general form of the Higgs potential, which affects the triple-quartic couplings in the scalar sector.

In the present work, the full set of one-loop contributions for the direct pair production of the pseudoscalar Higgs in a $\gamma\gamma$ collision is investigated in the framework of the THDM, taking into account both theoretical restrictions and experimental constraints from recent LHC data and other experimental results. Even though the same process in the framework of the THDM has already been analyzed in the literature, it still has rich physics results in terms of triple and quartic couplings and needs a detailed study in light of recent experimental constraints on the model parameters. However, in this work, the effects of individual contributions from each type of one-loop diagram on the total cross-section are analyzed in detail. Note that the results of the present study are consistent with those obtained in previous works.

The remainder of the paper is arranged as follows. In Section 2, a brief review is given for the THDM. Section 3 presents the experimental and theoretical constraints on the parameter space of the THDM and four benchmark point scenarios, which are consistent with these constraints. In Section 4, the corresponding one-loop Feynman diagrams are presented and analytical expressions for the production cross-section are briefly

reviewed. The numerical evaluation method is then explained. In Section 5, numerical results are presented and the model parameter dependencies of the cross-section are discussed in detail. Finally, in Section 6, the concluding remarks of the study are given.

2. A brief review of the two Higgs doublet model

For completeness, we first give a brief summary of the CP-conserving THDM here, including only those details relevant to this study. The interested reader can refer to [19] for a comprehensive review of these models.

The THDM is the most minimal extension of the SM containing extra Higgs doublet fields. In the THDM, the most general scalar potential can be written as:

$$\begin{aligned} V_{\text{THDM}} &= m_1^2|\Phi_1|^2 + m_2^2|\Phi_2|^2 - \left[m_{12}^2(\Phi_1^\dagger\Phi_2) + \text{h.c.}\right] \\ &+ \frac{\lambda_1}{2}(\Phi_1^\dagger\Phi_1)^2 + \frac{\lambda_2}{2}(\Phi_2^\dagger\Phi_2)^2 + \lambda_3(\Phi_1^\dagger\Phi_1)(\Phi_2^\dagger\Phi_2) + \lambda_4(\Phi_1^\dagger\Phi_2)(\Phi_2^\dagger\Phi_1) \\ &+ \left[\frac{\lambda_5}{2}(\Phi_1^\dagger\Phi_2)^2 + \lambda_6(\Phi_1^\dagger\Phi_1)(\Phi_1^\dagger\Phi_2) + \lambda_7(\Phi_1^\dagger\Phi_2)(\Phi_2^\dagger\Phi_2) + \text{h.c.}\right], \end{aligned} \tag{2.1}$$

where $\Phi_{1,2}$ are two complex scalar Higgs doublets and λ_i (i=1,...,7) are dimensionless quartic coupling parameters. To respect some low-energy observables, the discrete Z_2 symmetry proposed by the Paschos–Glashow–Weinberg theorem [20] is imposed to avoid flavor-changing neutral currents. As a result, the Z_2 symmetry requires that $\lambda_{6,7}$ and m_{12}^2 must be zero. However, letting m_{12}^2 be nonzero, this symmetry can be softly broken. The charges under this symmetry are assigned to ensure that each type of fermion couples to either Φ_1 or Φ_2. There are 4 types of THDMs, which are commonly called type-I, type-II, type-III, and type-IV THDMs, depending on the Z_2 assignment [4, 19]. The way in which each Higgs doublet ($\Phi_{1,2}$) couples to the fermions in the allowed types that naturally conserve flavor is given in Table 1.

Table 1. Couplings of u-type and d-type quarks and charged leptons to $\Phi_{1,2}$ in types allowed by the Z_2 symmetry. The subscript i is a generation index.

Type	u_i	d_i	ℓ_i
I	Φ_2	Φ_2	Φ_2
II	Φ_2	Φ_1	Φ_1
III	Φ_2	Φ_2	Φ_1
IV	Φ_2	Φ_1	Φ_2

Types III and IV are also known as "lepton-specific" and "flipped", respectively. In this study, the numerical analysis is carried out in the framework of the type-I THDM, in which only the doublet Φ_2 interacts with both quarks and leptons, like in the SM.

After electroweak symmetry breaking, each Φ acquires a vev v_j such that $v = \sqrt{v_1^2 + v_2^2} \approx 246$ GeV and

$$\Phi_j = \begin{pmatrix} \phi_j^+ \\ \frac{1}{\sqrt{2}}(v_j + \rho_j + i\eta_j) \end{pmatrix}, (j = 1, 2), \tag{2.2}$$

where ρ_j and η_j are real scalar fields. The two Higgs doublets initially have 8 degrees of freedom. Three of them (Goldstone bosons G^0, $G^\pm$) are absorbed by the longitudinal components of the electroweak gauge bosons

Z^0 and $W^\pm$. The remaining five are physical Higgs fields, a CP-odd A^0, two CP-even h^0 and H^0, and two charged scalars H^+ and H^-. The relevant mass eigenstates are determined by orthogonal transformations, in which the parameters β and α govern the mixing between mass eigenstates in the CP-odd/charged and CP-even sectors, respectively.

For any given value of $\tan\beta$, m_1^2 and m_2^2 are calculated by the minimization conditions of potential. The parameters $m_{1,2}^2$ and couplings λ_1–λ_5 may be expressed in terms of the physical masses $m_{h,H,A,H^\pm}$, along with $\tan\beta = v_2/v_1$, and $\sin(\beta-\alpha)$. The soft Z_2 symmetry breaking parameter m_{12}^2 can be written as

$$m_{12}^2 = \frac{1}{2}\lambda_5 v^2 \sin\beta\cos\beta = \frac{\lambda_5}{2\sqrt{2}G_F}\frac{\tan\beta}{1+\tan^2\beta}, \tag{2.3}$$

where the second equality is valid at tree level. Setting λ_6 and λ_7 to zero to respect the discrete Z_2 symmetry and working in the "physical basis", m_{12}^2, $\tan\beta$, mixing angle α, and four physical masses of the Higgs bosons can be used to specify the model completely. Consequently, in the Higgs sector of the THDM, there are seven independent parameters. From Eq. (2.1), the triple and quartic scalar couplings can be derived as a function of the masses m_{h^0}, m_{H^0}, m_{A^0}, $m_{H^\pm}$, and $\tan\beta$, α and m_{12}^2, as follows[2]:

$$\lambda^{THDM}_{h^0h^0h^0} = \frac{-3g}{2m_W s_{2\beta}^2}\left[(2c_{\alpha+\beta}+s_{2\alpha}s_{\beta-\alpha})s_{2\beta}m_{h^0}^2 - 4(c_{\beta-\alpha}^2 c_{\beta+\alpha})m_{12}^2\right], \tag{2.4}$$

$$\lambda^{THDM}_{H^0h^0h^0} = -\frac{gc_{\beta-\alpha}}{2m_W s_{2\beta}^2}\left[(2m_{h^0}^2+m_{H^0}^2)s_{2\alpha}s_{2\beta} - 2(3s_{2\alpha}-s_{2\beta})m_{12}^2\right], \tag{2.5}$$

$$\lambda^{THDM}_{h^0H^0H^0} = \frac{gs_{\beta-\alpha}}{2m_W s_{2\beta}^2}\left[(m_{h^0}^2+2m_{H^0}^2)s_{2\alpha}s_{2\beta} + 2(3s_{2\alpha}+s_{2\beta})m_{12}^2\right], \tag{2.6}$$

$$\lambda^{THDM}_{h^0A^0A^0} = \frac{g}{2m_W}\left[(m_{h^0}^2-2m_{A^0}^2)s_{\beta-\alpha} - \frac{2c_{\beta+\alpha}}{s_{2\beta}^2}(m_{h^0}^2 s_{2\beta}-2m_{12}^2)\right], \tag{2.7}$$

$$\lambda^{THDM}_{h^0H^\pm H^\mp} = \frac{g}{2m_W}\left[(m_{h^0}^2-2m_{H^\pm}^2)s_{\beta-\alpha} - \frac{2c_{\beta+\alpha}}{s_{2\beta}^2}(m_{h^0}^2 s_{2\beta}-2m_{12}^2)\right], \tag{2.8}$$

$$\lambda^{THDM}_{A^0G^0h^0} = \frac{gc_{\beta-\alpha}}{2m_W}\left[m_{A^0}^2-m_{h^0}^2\right], \quad \lambda^{THDM}_{A^0H^-G^+} = \frac{g}{2m_W}\left[m_{A^0}^2-m_{H^-}^2\right], \tag{2.9}$$

$$\begin{aligned}\lambda^{THDM}_{A^0A^0H^-H^+} = -\left(\frac{g}{2m_W s_{2\beta}}\right)^2\Big[&m_{H^0}^2(c_{\beta-\alpha}s_{2\beta}-2s_{\beta+\alpha})^2 + m_{h^0}^2(2c_{\beta+\alpha}-s_{2\beta}s_{\beta-\alpha})^2 \\ &+ 8\frac{m_{12}^2 c_{2\beta}^2}{s_{2\beta}}\Big],\end{aligned} \tag{2.10}$$

where the gauge coupling constant $g = e/sin\theta_W$ and m_W is the mass of boson W. These triple Higgs couplings are independent of the Yukawa types used because they follow from the scalar THDM potential. All

[2]The short-hand notations c_x and s_x are used for $\cos(x)$ and $\sin(x)$, respectively. For example, $c_{\alpha+\beta} = cos(\alpha+\beta)$ for $x = \alpha+\beta$.

these couplings have a strong dependence on the mixing angles α and β, the physical Higgs masses, and the soft breaking parameter m_{12}^2. In this study, in particular, triple Higgs couplings and couplings of the (pseudo)scalar to gauge bosons are of interest. The (pseudo)scalar–gauge couplings,

$$\begin{aligned} &\lambda_{h^0W^\pm W^\mp} = g m_W s_{\beta-\alpha},\ \lambda_{H^0W^\pm W^\mp} = g m_W c_{\beta-\alpha}, \\ &\lambda_{h^0G^\pm W^\mp} = \frac{g}{2} s_{\beta-\alpha},\ \lambda_{H^0G^\pm W^\mp} = \frac{g}{2} c_{\beta-\alpha}, \end{aligned} \tag{2.11}$$

are proportional to $c_{\beta-\alpha}$ or $s_{\beta-\alpha}$, while $\lambda_{A^0H^\pm W^\mp} = e/2s_W$ is independent of the THDM angles. Contrary to the CP-even h^0 and H^0, the pseudoscalar Higgs boson, due to its CP-odd nature, does not couple to pairs of ZZ and W^+W^-. Therefore, Z-boson and W-boson loop diagrams do not contribute to production of A^0 at the one-loop level.

In the THDM, a decoupling limit appears when $c_{\beta-\alpha} = 0$ and $m_{H^0,A^0,H^\pm} \gg m_Z$ [21]. In this limit, couplings of the Higgs boson h^0 to SM particles look entirely like the SM Higgs couplings, which include the coupling $h^0h^0h^0$. Furthermore, there is an alignment limit [22], where the Higgs boson h^0 (H^0) looks like the SM Higgs boson if $s_{\beta-\alpha} \to 1$ ($c_{\beta-\alpha} \to 1$). In the alignment or decoupling limit with $\alpha = \beta - \frac{\pi}{2}$, some triple couplings turn into the following forms:

$$\begin{aligned} \lambda_{h^0h^0h^0}^{THDM} &= \frac{-3g}{2m_W} m_{h^0}^2 = \lambda_{hhh}^{SM},\quad \lambda_{H^0h^0h^0}^{THDM} = 0, \\ \lambda_{h^0H^0H^0}^{THDM} &= \frac{g}{m_W}\left[\left(\frac{2m_{12}^2}{s_{2\beta}} - m_{H^0}^2\right) - \frac{m_{h^0}^2}{2}\right], \\ \lambda_{h^0A^0A^0}^{THDM} &= \frac{g}{m_W}\left[\left(\frac{2m_{12}^2}{s_{2\beta}} - m_{A^0}^2\right) - \frac{m_{h^0}^2}{2}\right], \\ \lambda_{h^0H^\pm H^\mp}^{THDM} &= \frac{g}{m_W}\left[\left(\frac{2m_{12}^2}{s_{2\beta}} - m_{H^\pm}^2\right) - \frac{m_{h^0}^2}{2}\right]. \end{aligned} \tag{2.12}$$

3. Parameter setting and constraints on the THDM

The parameter space of the THDM potential is decreased by the results of experimental studies as well as by theoretical constraints. The THDM is subjected to several theoretical restrictions such as potential stability, perturbativity, and unitarity. For ensuring vacuum stability of the THDM, V_{THDM} must be bounded from below. In other words, $V_{\text{THDM}} \geq 0$ must be maintained for all directions of Φ_1 and Φ_2. This constraint puts the following conditions on the parameters λ_i [23–25]:

$$\begin{aligned} &\lambda_1 > 0, \quad \lambda_2 > 0, \\ &\lambda_3 + 2\sqrt{\lambda_1\lambda_2} > 0, \\ &\lambda_3 + \lambda_4 - |\lambda_5| > 2\sqrt{\lambda_1\lambda_2}. \end{aligned} \tag{3.1}$$

There is also another set of constraints that imposes that perturbative unitarity must be satisfied for the scattering of longitudinally polarized gauge bosons and Higgs bosons. This can be seen in [26–29]. Furthermore, the scalar potential must be perturbative by imposing that all λ_i satisfy $|\lambda_{1,2,3,4,5}| \leq 8\pi$.

Besides the above theoretical constraints, the THDM has current constraints resulting from direct observations at the LHC and indirect experimental limits from B physics observables. In the type-I THDM,

pseudoscalar Higgs mass regions such as $310 < m_A < 410$ GeV for $m_H = 150$ GeV, $335 < m_A < 400$ GeV for $m_H = 200$ GeV, and $350 < m_A < 400$ GeV for $m_H = 250$ GeV at $tan\beta = 10$ have been excluded by the LHC experiment [30]. Moreover, the limit $m_A > 350$ is put on the pseudoscalar Higgs mass for $tan\beta < 5$ [31] and the mass range $170 < m_H < 360$ GeV is excluded for $tan\beta < 1.5$ in the type-I model [32].

In type-II and type-IV THDM, the data from the measurement of the branching ratio $b \to s\gamma$ put constraints on the charged Higgs mass $m_{H^\pm} > 580$ GeV [33, 34] for $tan\beta \geq 1$. However, for the other types of THDM, this bound is much lower [35]. In type-I and type-III THDM, as long as $tan\beta \geq 2$, the charged Higgs bosons can be as light as 100 GeV [35, 36] while being compatible with LHC and LEP bounds as well as with all B physics restrictions [37–42]. Moreover, there is no exclusion around $sin(\beta - \alpha) = 1$ for $m_{A,H^0,H^\pm} = 500$ GeV in the type-I THDM according to a review of LEP, LHC, and Tevatron results [43].

In this study, 4 benchmark point (BP) scenarios are chosen as shown in Table 2. These are consistent with experimental and theoretical constraints. The BPs are constructed on the type-I THDM with an alignment limit $s_{\beta-\alpha} \to 1$, and hence the CP-even Higgs h^0 is a SM-like Higgs. Its mass is fixed as $m_h = 125.18$ GeV [44]. The value of $\tan\beta$ is set to 10 for all benchmark scenarios, which results in a remarkable enhancement in the assumed scalar Higgs boson decay channel.

Table 2. Selected BPs using Higgs data for type-I THDM with alignment limit. All BPs are still allowed by searches for additional Higgs bosons at the LHC.

BPs	m_{h^0} (GeV)	m_{A^0} (GeV)	m_{H^0} (GeV)	$m_{H^\pm}$ (GeV)	m_{12}^2 (GeV^2)	$\tan\beta$	$\sin(\beta-\alpha)$
BP1	125.18	150	150	150	2000	10	1
BP2		200	150	250	2000		
BP3		250	150	250	2000		
BP4		250	250	300	6000		

The potential stability, perturbativity, and unitarity of each BP have been checked with the help of `2HDMC 1.7.0` [45, 46]. The considered benchmark scenarios are also consistent with the bounds derived from different studies on extra Higgs bosons at the LHC, provided that h^0 ought to provide the properties of the observed Higgs boson. The constraints are checked by `HiggsBounds 4.3.1` [47] and `HiggsSignals 1.4.0` [48] with the results of 86 analyses.

Table 3. The dominant branching ratios (BRs) of CP-odd Higgs A^0 for selected BPs, where BRs values of less than 10^{-4} are not shown.

	BP1	BP2	BP3	BP4
BR($A^0 \to gg$)	3.06×10^{-1}	1.67×10^{-1}	0.09×10^{-2}	5.93×10^{-1}
BR($A^0 \to b\bar{b}$)	6.03×10^{-1}	1.78×10^{-1}	0.05×10^{-2}	3.49×10^{-1}
BR($A^0 \to c\bar{c}$)	2.78×10^{-2}	0.81×10^{-2}	$< 10^{-4}$	1.61×10^{-2}
BR($A^0 \to \tau^+\tau^-$)	6.15×10^{-2}	1.92×10^{-2}	$< 10^{-4}$	3.94×10^{-2}
BR($A^0 \to Z^0H^0$)	–	6.28×10^{-1}	9.98×10^{-1}	–

The dominant branching ratios of A^0, which are computed by using `2HDMC 1.7.0`, are listed for selected BPs in Table 3. The most dominant ratios are shaded in blue: $A^0 \to b\bar{b}$ for BP1, $A^0 \to Z^0H^0$ for BP2 and BP3, and $A^0 \to gg$ for BP4.

4. Analytical expressions for the production cross-section

The pseudoscalar-Higgs boson A^0 pair production via photon–photon collision is denoted by

$$\gamma(p_1)\gamma(p_2) \to A^0(k_1)A^0(k_2), \tag{4.1}$$

where after each particle, as usual, its 4-momentum is written in parentheses. This subprocess has no amplitude at tree level, and it has one-loop level amplitude in the lowest order. A full set of one-loop level Feynman diagrams[3] contributing to process 4.1 in the THDM is generated by `FeynArts` [50, 51]. They are shown in Figures 1–3. The process also has another set of Feynman diagrams that are not given in the figures where particles in loops are flowing in the opposite direction. The square bracket $[G, W]$ means that the loop contains all possible combinations of particles G and W.

Any one-loop amplitude is composed of a sum over the following integrals with up to n propagators carrying loop momentum:

$$T^n_{\mu_1\ldots\mu_s} = \frac{\mu^{4-d}}{i\pi^{d/2}\, r_\Gamma} \int d^d q \, \frac{q_{\mu_1}\cdots q_{\mu_s}}{\left[q^2 - m_1^2\right]\left[(q+k_1)^2 - m_2^2\right]\cdots\left[(q+k_{n-1})^2 - m_n^2\right]}, \tag{4.2}$$

where $r_\Gamma = \Gamma^2(1-\varepsilon)\Gamma(1+\varepsilon)/\Gamma(1-2\varepsilon)$, $d = 4-2\varepsilon$, and s is the number of qs in the numerator, which specifies the Lorentz tensor structure of all integrals ($s = 0$ indicates a scalar integral, $s = 1$ a vector integral, etc.). The denominator emerges from the propagators of the particles in the loop. The parameter μ is a renormalization scale, which keeps the integral's mass dimension the same in all d-dimensions. In the case that the integrals involve infrared and ultraviolet divergences, dimensional regularization [52] is used, analytically continuing the loop momentum integral to d dimensions. According to the Passarino-Veltman reduced method [53], the integral with a tensor structure can be reduced to linear combinations of Lorentz covariant tensors constructed from a linearly independent set of the momentum and the metric tensor $g_{\mu\nu}$. Consequently, any amplitude at one-loop level can be written as a linear sum of one-loop integrals such as bubble, box, triangle, and tadpole.

According to the loop-correction type, the diagrams of $\gamma\gamma \to A^0A^0$ at one-loop level can be classified into three groups, which are called triangle-type, box-type, and quartic-type diagrams. Figure 1 shows all box-type diagrams, which have the loops of charged-leptons and quarks, bosons of $G^\pm$, $W^\pm$, and $H^\pm$. These are t- and u-channel diagrams. Figure 2 shows all triangle-type diagrams, which consist of triangle vertices (t_{1-4}) attached to the final state via intermediate Higgs bosons h^0 or H^0. Finally, Figure 3 shows all quartic coupling-type diagrams. They include bubbles (q_{1-3}) attached to the final state via intermediate Higgs bosons h^0 or H^0, bubbles loop (q_{4-6}) and triangle loop (q_7, q_{14}) of bosons $G^\pm$, $H^\pm$, and $W^\pm$ directly attached to the final state. The diagrams t_{1-4} and q_{1-3} are s-channel diagrams. The resonant effects appear only in the triangle diagrams (t_{1-4}) and in the bubbles type (q_{1-3}) due to the intermediate neutral Higgs bosons.

Note that the Feynman diagrams of the processes $\gamma\gamma \to H^0H^0$ and $\gamma\gamma \to H^0A^0$ are almost the same as those of the $\gamma\gamma \to A^0A^0$ considered in this study. Therefore, any result to be obtained for the process $\gamma\gamma \to A^0A^0$ can be also applied to these processes, depending on the parameters of the model.

Table 4 shows the triple/quartic Higgs couplings and couplings of the (pseudo)scalar to the W-boson, which are included in each type of diagram. Feynman diagrams are dominated by triple couplings $\lambda_{H^+G^-A^0}$ and $\lambda_{H^+W^-A^0}$, which are independent of the THDM angles. Owing to the CP nature of A^0, the box-type diagrams

[3]Note that Feynman diagrams have been plotted by using `JaxoDraw` [49].

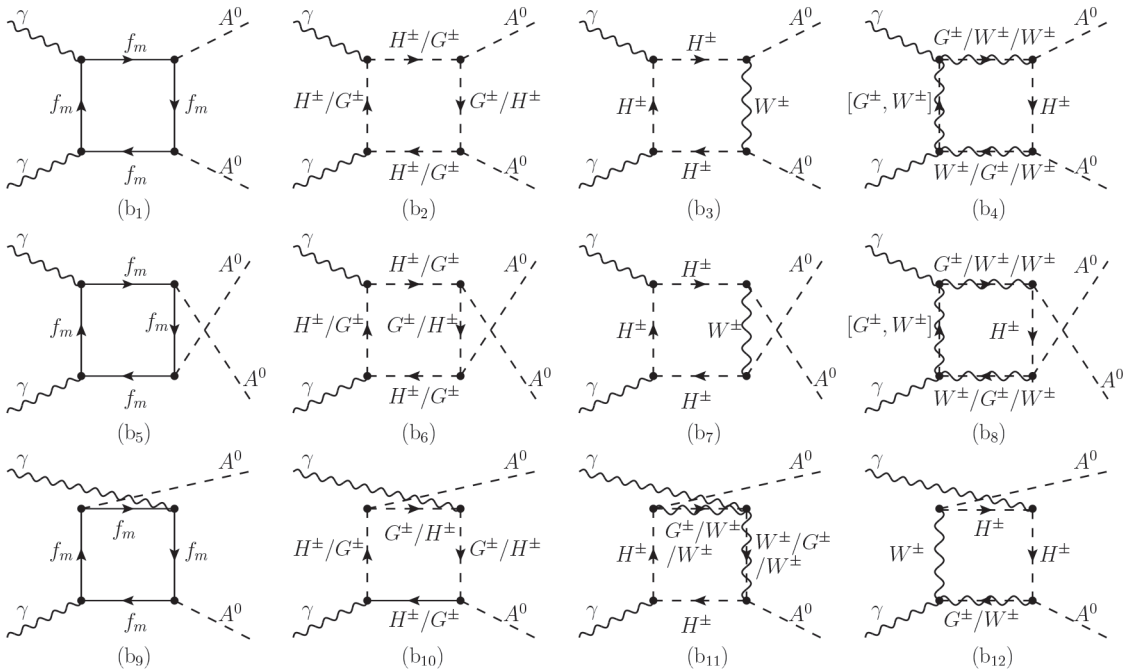

Figure 1. Box-type diagrams for $\gamma\gamma \to A^0A^0$. Here, the label f_m represents fermions of $e, \mu, \tau, u, d, c, s, t$, and b.

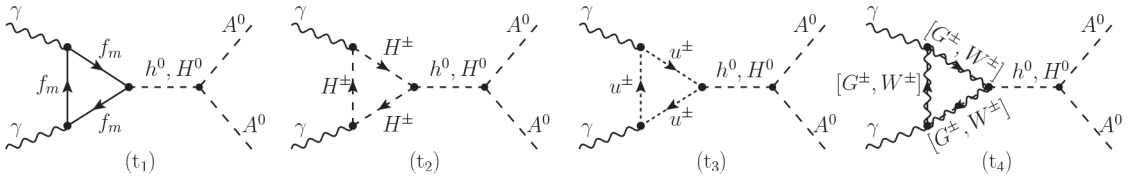

Figure 2. Triangle-type diagrams for $\gamma\gamma \to A^0A^0$. Here, the label f_m refers to fermions of $e, \mu, \tau, u, d, c, s, t$, and b.

are rather sensitive to the coupling $\lambda_{H^+G^-A^0}$, which has neither a $\tan\beta$ nor a m_{12}^2 dependence. Triple couplings $\lambda_{[h^0,H^0]A^0A^0}$, $\lambda_{H^+H^-[h^0,H^0]}$, and $\lambda_{G^+G^-[h^0,H^0]}$ only appear in s-channel diagrams and they are amplified by resonance effects due to neutral Higgs bosons. Diagrams q_4, q_7 and q_8 in Figure 3 are sensitive to quartic couplings $\lambda_{H^+H^-A^0A^0}$ and $\lambda_{G^+G^-A^0A^0}$, which are proportional to mixing angles and the mass parameter m_{12}^2.

The one-loop amplitude of the process $\gamma\gamma \to A^0A^0$ could be computed by summing all unrenormalized reducible and irreducible contributions. Consequently, finite and gauge invariant results can be obtained. Therefore, renormalization is not required for ultraviolet divergence. The corresponding matrix element[4] is calculated as a sum over all contributions:

$$\mathcal{M} = \mathcal{M}_{box} + \mathcal{M}_{quartic} + \mathcal{M}_{bubble} + \mathcal{M}_{triangle}, \tag{4.3}$$

where a relative sign $(-1)^{\delta_{ij}}$ is written between one diagram and its counterpart emerging by interchanging

[4]In this study, an expression of the matrix element is not explicitly presented because it is too lengthy to include here.

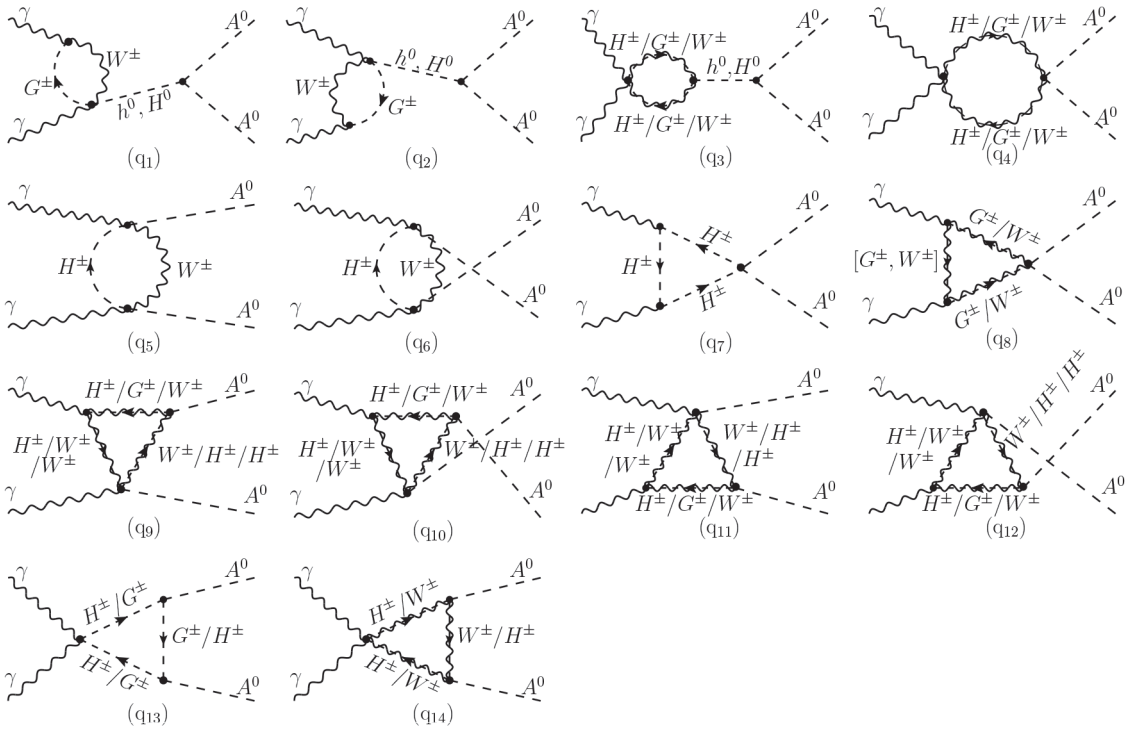

Figure 3. Quartic interaction diagrams for $\gamma\gamma \to A^0A^0$.

Table 4. Triple/quartic Higgs couplings and couplings of the (pseudo)scalar to the W-boson, which are included in each type of diagram.

	Couplings	Box-type	Triangle-type	Bubble-type	Quartic-type
SSS	$\lambda_{[h^0,H^0]A^0A^0}$		✓($t_{1,2,3,4}$)	✓($q_{1,2,3}$)	
	$\lambda_{H^+H^-[h^0,H^0]}$		✓(t_2)	✓(q_3)	
	$\lambda_{G^+G^-[h^0,H^0]}$		✓(t_4)	✓(q_3)	
	$\lambda_{H^+G^-A^0}$	✓($b_{2,4,6,8,10,11,12}$)			✓($q_{9,10,11,12,13}$)
WSS WWS	$\lambda_{H^+W^-A^0}$	✓($b_{3,4,7,8,11,12}$)			✓($q_{9,10,11,12,14}$)
	$\lambda_{W^+W^-[h^0,H^0]}$		✓(t_4)	✓(q_3)	
	$\lambda_{G^+W^-[h^0,H^0]}$		✓(t_4)		
SSSS WWSS	$\lambda_{H^+H^-A^0A^0}$			✓(q_4)	✓(q_7)
	$\lambda_{G^+G^-A^0A^0}$			✓(q_4)	✓(q_8)
	$\lambda_{W^+W^-A^0A^0}$			✓(q_4)	✓(q_8)

the final states. The total cross-section of $\gamma\gamma \to A^0A^0$ is given by

$$\hat{\sigma}(\hat{s}_{\gamma\gamma}, \gamma\gamma \to A^0A^0) = \frac{1}{32\pi\hat{s}_{\gamma\gamma}^2}\int_{\hat{t}^-}^{\hat{t}^+} d\hat{t}\overline{\sum}|\mathcal{M}|^2, \tag{4.4}$$

where

$$\hat{t}^{\pm} = (m_A^2 - \hat{s}_{\gamma\gamma}/2) \pm \left(\sqrt{(\hat{s}_{\gamma\gamma} - 2m_A^2)^2 - 4m_A^4}\right)/2. \tag{4.5}$$

The $\gamma\gamma$ collision can be performed at the facility of the next generation of TeV-class linear colliders such as the CLIC and the ILC. Then $\gamma\gamma \to A^0A^0$ is produced as a subprocess of e^-e^+ collision at the linear colliders. The total cross-section of $e^+e^- \to \gamma\gamma \to A^0A^0$ could be obtained by folding $\hat{\sigma}(\gamma\gamma \to A^0A^0)$ with the photon luminosity

$$\frac{dL_{\gamma\gamma}}{dz} = 2z \int_{z^2/x_{max}}^{x_{max}} \frac{dx}{x} F_{\gamma/e}(x) F_{\gamma/e}\left(\frac{z^2}{x}\right), \tag{4.6}$$

as follows:

$$\sigma(s, e^+e^- \to \gamma\gamma \to A^0A^0) = \int_{(2m_{A^0})/\sqrt{s}}^{x_{max}} dz \frac{dL_{\gamma\gamma}}{dz}\, \hat{\sigma}(\gamma\gamma \to A^0A^0;\ \hat{s}_{\gamma\gamma} = z^2 s), \tag{4.7}$$

where $F_{\gamma/e}(x)$ is the photon structure function. The photon spectrum is qualitatively better for larger values of the x-fraction of the longitudinal momentum of the e^--beam. However, for $x > 2(1+\sqrt{2}) \approx 4.8$, the high-energy photons could disappear through the pair production of e^-e^+ in its collision with a following laser-γ. The energy spectrum of the photon supplied as a Compton backscattered photon off the electron beam [54] is used for the photon structure function of this study.

The numerical evaluation for both $\gamma\gamma \to A^0A^0$ and $e^+e^- \to \gamma\gamma \to A^0A^0$ is carried out by the help of Mathematica packages as follows: the relevant amplitudes are generated by `FeynArts` [50], the analytical expressions of the squared matrix elements are provided by `FormCalc` [55], and the necessary one-loop scalar integrals are evaluated by `LoopTools` [56]. Note that ultraviolet divergences for the general one loop-integral 4.2 are dimensionally regularized by `LoopTools`. UV-divergent loop integrals include the combination $1/\varepsilon - \gamma_{\rm E} + \log 4\pi$, for which `LoopTools` puts the actual divergence into the ε^{-1} component of the result and substitutes the finite part by Δ. `LoopTools` provides ways to numerically check for the cancellation of divergences. The integration over the phase space of $2 \to 2$ is numerically evaluated by using the CUBA library. For the photon structure function, Compton backscattered photons, which are interfaced by the `CompAZ` code [57], are used. Using the tools described above, we have previously carried out several works and found significant results [58, 59].

5. Numerical results and discussion

The numerical predictions for the direct pair production of the pseudoscalar Higgs boson at a $\gamma\gamma$ collision are presented in detail, taking into account a full set of one-loop level Feynman diagrams. During our calculations, the cancellation of divergences appearing in the loop contributions has been numerically checked. The finite results have been obtained without the need for the renormalization procedure. The integrated cross-section $\hat{\sigma}(\gamma\gamma \to A^0A^0)$ is analyzed as a function of the center-of-mass energy $\sqrt{\hat{s}_{\gamma\gamma}}$, focusing on the individual contributions from each type of diagram and on the polarization configurations of the incoming photons for representative BPs given in Table 2. The dependencies of $\hat{\sigma}(\gamma\gamma \to A^0A^0)$ on the plane of $m_{12}^2 - \tan\beta$ and $m_A - \tan\beta$ are also investigated. Furthermore, $\sigma(e^+e^- \to \gamma\gamma \to A^0A^0)$ is numerically evaluated as a function of $\sqrt{s}$ (for BPs given in Table 2) and m_A for several Higgs mass hierarchies.

In Figure 4, the contribution of each type of diagram to $\hat{\sigma}(\gamma\gamma \to A^0A^0)$ is shown as a function of $\sqrt{\hat{s}_{\gamma\gamma}}$ for each benchmark point. The labels "box", "tri", "bub", "qua", and "all" represent the box-type contribution ($\mathrm{b}_{1\to12}$), triangle-type contribution ($\mathrm{t}_{1\to4}$), bubble-type contribution ($\mathrm{q}_{1\to6}$), quartic-type

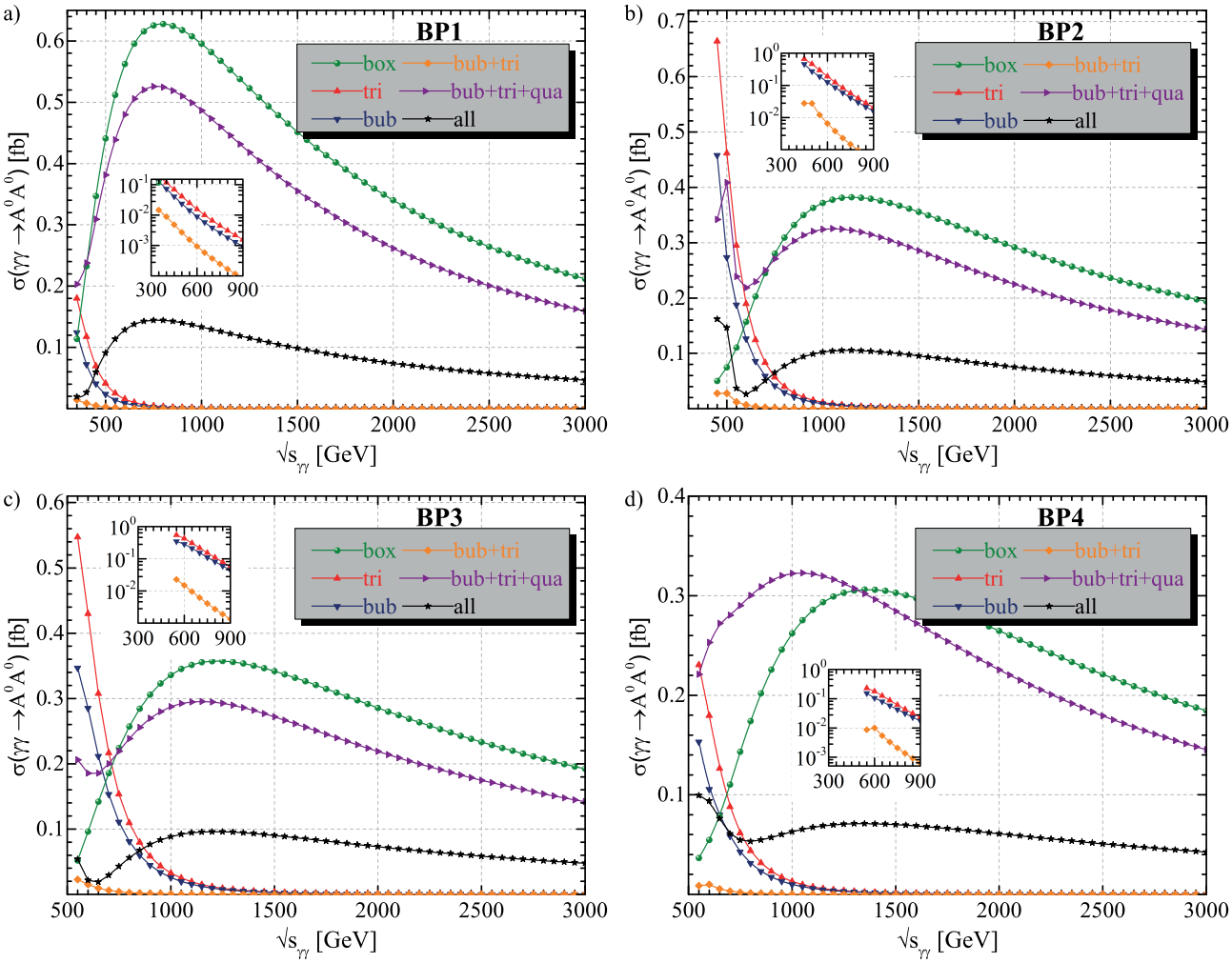

Figure 4. The individual contributions from each type of diagram to total cross-section of process $\gamma\gamma \to A^0A^0$ as a function of center-of-mass energy for each benchmark point. The inset figures show the contributions of the triangle-type, bubble-type, and their interference in the center-of-mass energy range of 300–900 GeV.

contribution ($q_{7\to14}$), and all diagrams' contributions, respectively. Additionally, "bub+tri" corresponds to the contribution resulting from interference of the bubble type with triangle-type diagrams. For each of the BPs, the integrated cross-section $\hat{\sigma}(\gamma\gamma \to A^0A^0)$ is enhanced by the threshold effect when $\sqrt{\hat{s}}_{\gamma\gamma}$ is close to 2 times the mass of charged Higgs $H^{\pm}$, because the production process $\gamma\gamma \to H^+H^-$ is open at this threshold energy. Note that contributions from bubble-type and triangle-type diagrams, which are also called s-channel contributions, are suppressed at the high energies owing to the s-channel propagator. However, the resonant effects can also be seen in these diagrams because of the intermediate neutral Higgs bosons. Particularly, at low center-of-mass energies, $\hat{\sigma}(\gamma\gamma \to A^0A^0)$ is dominated by triangle-type diagrams since the couplings $h^0A^0A^0$ and $h^0H^+H^-$ are large.

At high center-of-mass energy, where the triangle-type contributions are suppressed, $\hat{\sigma}(\gamma\gamma \to A^0A^0)$ is dominated by the box-type contributions. However, the bubble-type and triangle-type contributions are almost equal, and their interference (bub+tri) makes a much smaller contribution compared to each of them (by one

to two orders of magnitude) for all BPs because they nearly destroy each other. This means that they exert a destructive interference. Additionally, the box-type contribution is larger than the interference contribution of (bub+tri). Though the quartic-type interactions provide a positive contribution to the total cross-section, the sum of the diagrams of quartic type, bubble type, and triangle type (bub+tri+qua) still makes a smaller contribution than the box-type diagrams.

The size of $\hat{\sigma}(\gamma\gamma \to A^0A^0)$ is at a visible level of 10^{-1} fb for selected BPs. Furthermore, it is sorted according to BPs as $\hat{\sigma}\,(\mathrm{BP1}) > \hat{\sigma}\,(\mathrm{BP2}) > \hat{\sigma}\,(\mathrm{BP3}) > \hat{\sigma}\,(\mathrm{BP4})$. The basic size of $\hat{\sigma}(\gamma\gamma \to A^0A^0)$ differs by 1–2 orders of magnitude depending on the triple and quartic couplings of the pseudoscalar Higgs boson produced.

In Figure 5, the integrated cross-section of process $\gamma\gamma \to A^0A^0$ is given for various polarization configurations of the incoming photons, which are both right-handed RR polarized and opposite polarization RL. Note that cross-sections are equal in the case of the following polarizations: $\hat{\sigma}(RR) = \hat{\sigma}(LL)$ and $\hat{\sigma}(RL) = \hat{\sigma}(LR)$.

The unpolarized cross-section reaches up to 0.14 fb in BP1 at $\sqrt{\hat{s}}_{\gamma\gamma} = 750$ GeV, 0.11 fb in BP2 at $\sqrt{\hat{s}}_{\gamma\gamma} = 1150$ GeV, 0.096 fb in BP3 at $\sqrt{\hat{s}}_{\gamma\gamma} = 1200$ GeV, and 0.07 fb in BP4 at $\sqrt{\hat{s}}_{\gamma\gamma} = 1350$ GeV, and then

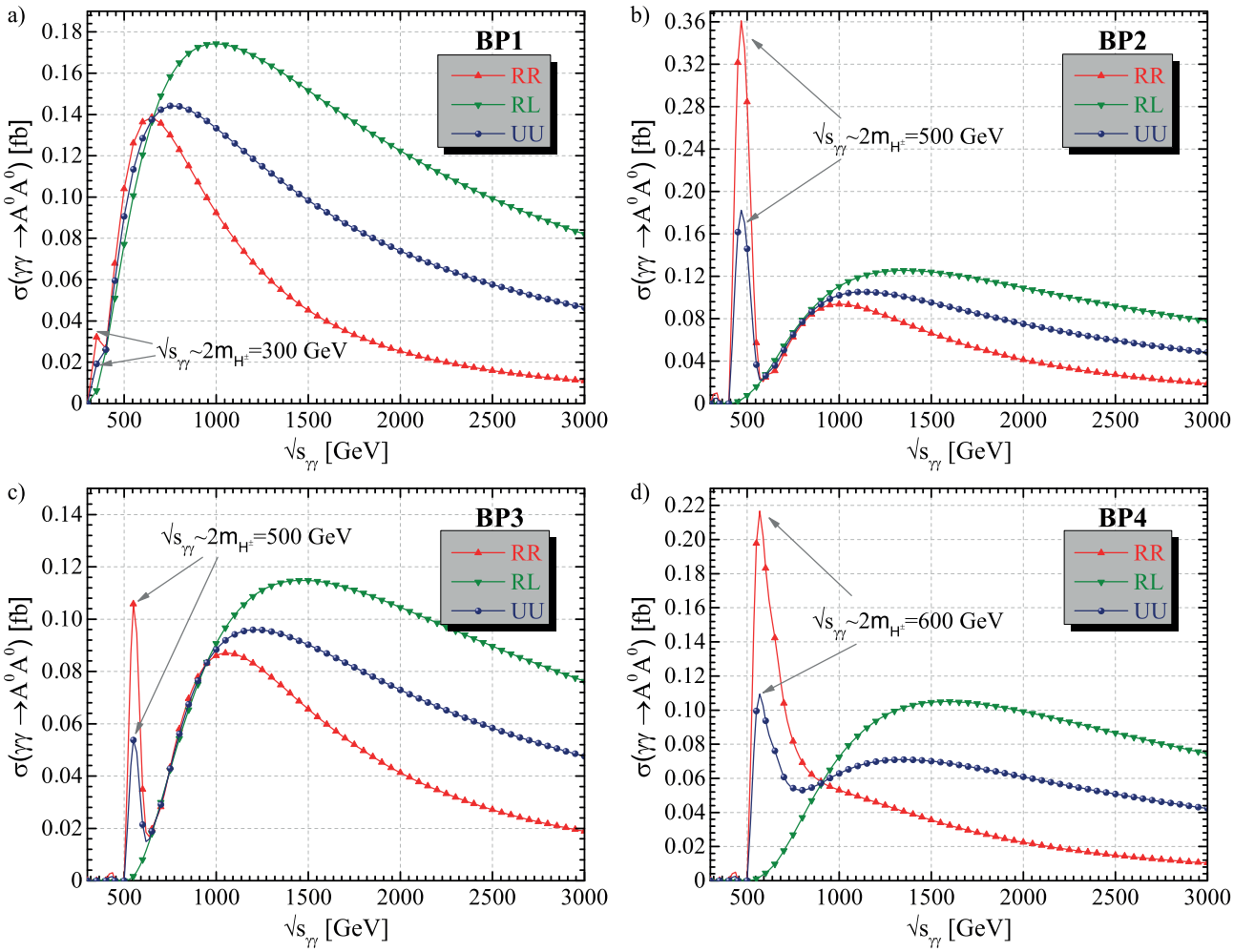

Figure 5. The total cross-section of process $\gamma\gamma \to A^0A^0$ as a function of center-of-mass energy for each benchmark point. The threshold effects are shown with arrows. UU, RR, and RL indicate situations of two photons with unpolarization, right polarization, and opposite polarization, respectively.

it falls for all cases. For high center-of-mass energies where the threshold effects disappear, when the initial photons have LR or RL polarizations, the total cross-section is amplified by a factor of two as compared to the unpolarized case (UU). The threshold effect is observed in the case of two photons with left-handed (LL) or right-handed (RR) polarization but not in the case of opposite polarization (LR) or (RL).

It is well known that the triple and quartic couplings of the pseudoscalar Higgs boson to other particles depend on the soft breaking parameter m_{12}^2, m_A, and $\tan\beta$. These parameter dependencies of the cross-section can provide important information about these couplings. From these dependencies, one can reveal a region of the parameter space where the increment of the cross-section is high enough to be detectable at future linear colliders. In respect to this, the integrated cross-section of $\gamma\gamma \to A^0A^0$ is scanned over the regions of $m_{12}^2 - \tan\beta$ and $m_A - \tan\beta$ at $\sqrt{\hat{s}} = 1$ TeV, as shown in Figures 6a and 6b.

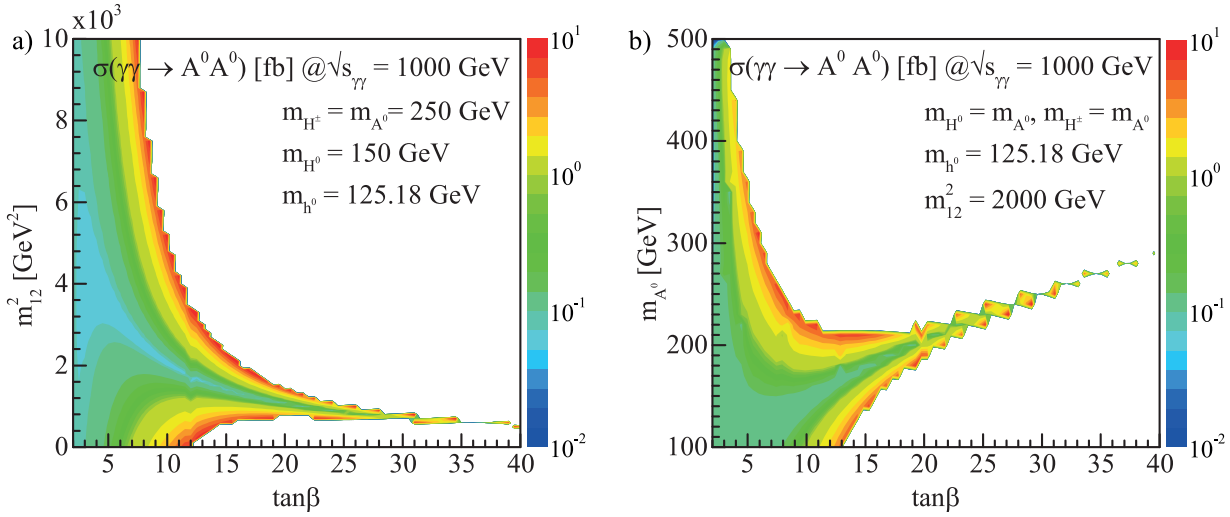

Figure 6. The total cross-section of process $\gamma\gamma \to A^0A^0$ as a 2D function of parameters (a) $m_{12}^2 - \tan\beta$ and (b) $m_A - \tan\beta$ for $\sqrt{\hat{s}} = 1$ TeV. The color heat map corresponds to the total cross-section in the scan region. The white region represents parameter space in which production of A^0A^0 is kinematically unavailable as well as not allowed by theoretical constraints.

The scan parameters are varied as follows: $0 \leq m_{12}^2 \leq 10^4$ GeV^2 in steps of 100 GeV, $100 \leq m_A \leq 500$ GeV in steps of 10 GeV, and $2 \leq \tan\beta \leq 40$ in steps of 0.5. However, most of parameter region is reduced by theoretical constraints as well as due to being kinematically inaccessible. The cross-section is enhanced at the border of the allowed and not-allowed regions. The size of $\sigma(\gamma\gamma \to A^0A^0)$ is at a visible level of 10^{-1} to 10^1 fb for the considered parameter regions.

Finally, Figure 7 shows the dependence of $\sigma(e^+e^- \to \gamma\gamma \to A^0A^0)$ on the center-of-mass energy for each BP and pseudoscalar Higgs mass for several Higgs mass hierarchies. $\sigma(e^-e^+ \to \gamma\gamma \to A^0A^0)$ is evaluated by convoluting $\sigma(\gamma\gamma \to A^0A^0)$ with the photon luminosity spectrum-based Compton backscattered photons. It can be easily seen that the total cross-section in the BP1 scenario is larger than the others. The total cross-section is enhanced by the threshold effect when $0.83\sqrt{s} \sim 2m_{H^\pm}$, because the production process $\gamma\gamma \to H^+H^-$ is kinematically open at this energy. The size of $\sigma(e^-e^+ \to \gamma\gamma \to A^0A^0)$ is at a visible level of 10^{-2} to 10^{-3} fb, depending on BPs. For selected BPs, the pseudoscalar Higgs boson pair production is more likely to be observed in the $\gamma\gamma$ collider than in the e^-e^+ collider. Total cross-section decreases with increasing pseudoscalar

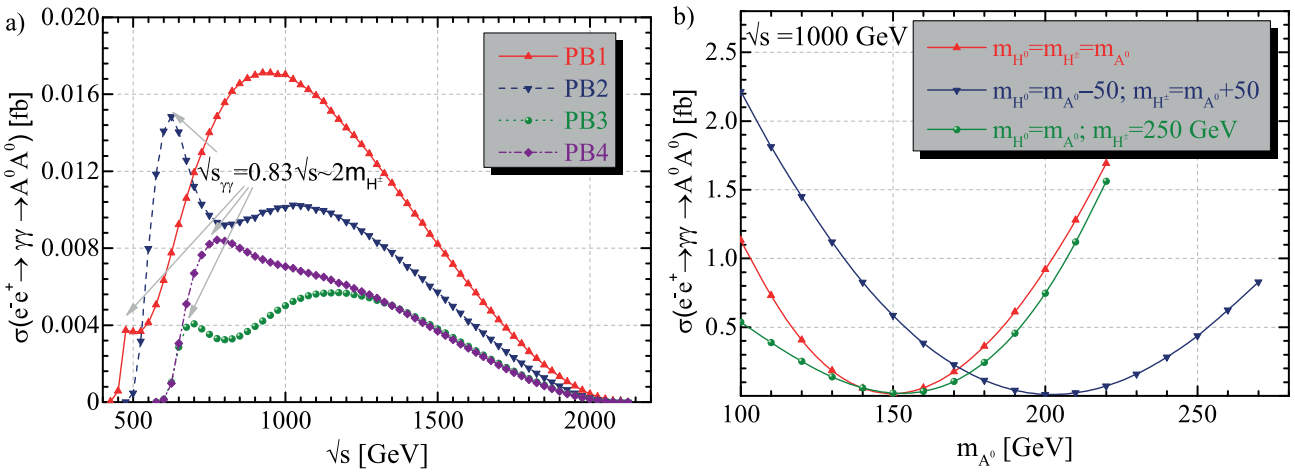

Figure 7. The total cross-section of process $e^-e^+ \to \gamma\gamma \to A^0A^0$ as a function of (a) center-of-mass energy for each benchmark point and (b) pseudoscalar Higgs mass for different Higgs mass hierarchies.

Higgs mass up to a certain threshold, and then it increases due to the resonant effects. In particular, the total cross-section reaches a value of 2.22 fb for $m_{A^0} = 100$ GeV in the case of $m_{H^\pm} = m_{H^0} = m_{A^0}$.

6. Conclusion

In this study, the process $\gamma\gamma \to A^0A^0$, nonexistent at tree level and first appearing at one-loop level, has been studied with special emphasis put on individual contributions from each type of diagram at a $\gamma\gamma$ collider as well as an electron–positron collider. Numerical evaluation has been carried out in the framework of the THDM, taking into account both theoretical restrictions and experimental constraints from recent LHC data and other experimental results. The energy-dependent structure of the cross-section is revealed by resonance effects owing to the intermediate neutral Higgs boson as well as by the threshold effect when $\sqrt{s_{\gamma\gamma}} \sim 2m_{H^\pm}$. For all cases, the box-type diagrams make dominant contributions at high energies. Owing to the CP nature of A^0, the box-type diagrams are rather sensitive to the coupling $\lambda_{H^\pm G^\mp A^0}$, which has neither a $\tan\beta$ nor a m_{12}^2 dependence. Hence, the process $\gamma\gamma \to A^0A^0$ can allow detection of the coupling $\lambda_{H^\pm G^\mp A^0}$. However, triple couplings $\lambda_{[h^0,H^0]A^0A^0}$, $\lambda_{H^+H^-[h^0,H^0]}$, and $\lambda_{G^+G^-[h^0,H^0]}$ only appear in s-channel diagrams and they can be amplified by resonance effects due to neutral Higgs bosons. The polarization configurations of the initial photons have the potential to amplify the total cross-sections. Consequently, the cross-section of the pair production of the pseudoscalar Higgs boson at a photon–photon collision could be considerably amplified in the THDM and therefore the expected number of events at a $\gamma\gamma$ collider can allow us to determine or exclude the parameter space of the THDM potential.

References

[1] Aad G, Abajyan T, Abbott B, Abdallah J, Abdel Khalek S et al. Observation of a new particle in the search for the Standard Model Higgs boson with the ATLAS detector at the LHC. Physics Letters B 2012; 716: 1-29. doi: 10.1016/j.physletb.2012.08.020

[2] Chatrchyan S, Khachatryan V, Sirunyan AM, Tumasyan A, Adam W et al. Observation of a new boson at a mass of 125 GeV with the CMS experiment at the LHC. Physics Letters B 2012; 716: 30-61. doi: 10.1016/j.physletb.2012.08.021

[3] Aad G, Abbott B, Abdallah J, Abdinov O, Abeloos B et al. Measurements of the Higgs boson production and decay rates and constraints on its couplings from a combined ATLAS and CMS analysis of the LHC pp collision data at $\sqrt{s} = 7$ and 8 TeV. Journal of High Energy Physics 2016; 2016 (8): 45. doi: 10.1007/JHEP08(2016)045

[4] Gunion JF, Haber HE, Kane GL, Dawson S. The Higgs Hunter's Guide. Upton, NY, USA: Brookhaven National Laboratory, 1990.

[5] Haber HE, Kane GL. The search for supersymmetry: probing physics beyond the standard model. Physics Reports 1985; 117: 75-263. doi: 10.1016/0370-1573(85)90051-1

[6] Behnke T, Brau JE, Foster B, Fuster J, Harrison M et al. The International Linear Collider Technical Design Report-Volume 1: Executive Summary. Report No. ILC-REPORT-2013-040. arXiv: 1306.6327 [physics.acc-ph].

[7] Baer H, Barklow T, Fujii K, Gao Y, Haong A et al. The International Linear Collider Technical Design Report-Volume 2: Physics, Report No. ILC-REPORT-2013-040. arXiv: 1306.6352 [hep-ph].

[8] Linssen L, Miyamoto A, Stanitzki M, Weerts H. Physics and Detectors at CLIC: CLIC Conceptual Design Report. Report No. CERN-2012-003. arXiv: 1202.5940 [physics.ins-det].

[9] Yamamoto A. International Linear Collider (ILC) - Technical Progress and Prospect. In: PoS: 38th International Conference on High Energy Physics; Chicago, IL, USA; 2016. doi: doi.org/10.22323/1.282.0067

[10] Aihara H, Bagger J, Bambade P, Barish B, Behnke T et al. The International Linear Collider: A Global Project. arXiv: 1901.09829 [hep-ex].

[11] Fujii K, Grojean C, Peskin ME, Barklow T, Gao Y et al. The Potential of the ILC for Discovering New Particles. Report No. DESY-17-012. KEK-PREPRINT-2016-60. arXiv: 1702.05333 [hep-ph].

[12] Gunion JF, Haber HE. Higgs boson production in the photon-photon collider mode of a high-energy e+ e- linear collider. Physical Review D 1993; 48: 5109-5120. doi: 10.1103/PhysRevD.48.5109

[13] Muhlleitner MM, Kramer M, Spira M, Zerwas PM. Production of MSSM Higgs bosons in photon photon collisions. Physics Letters B 2001; 508: 311-316. doi: 10.1016/S0370-2693(01)00321-5

[14] Asner DM, Gronberg JB, Gunion JF. Detecting and studying Higgs bosons in two-photon collisions at a linear collider. Physical Review D 2003; 67: 035009. doi: 10.1103/PhysRevD.67.035009

[15] Hodgkinson RN, Lopez-Val D, Sola J. Higgs boson pair production through gauge boson fusion at linear colliders within the general 2HDM. Physics Letters B 2009; 673: 47-56. doi: 10.1016/j.physletb.2009.02.009

[16] Arhrib A, Benbrik R, Chiang CW. Probing triple Higgs couplings of the two Higgs doublet model at Linear Collider. Physical Review D 2008; 77: 115013. doi: 10.1103/PhysRevD.77.115013

[17] Arhrib, A, Benbrik R, Chen CH, Santos R. Neutral Higgs boson pair production in photon-photon annihilation in the two Higgs doublet model. Physical Review D 2009; 80: 015010. doi: 10.1103/PhysRevD.80.015010

[18] Hernández-Sánchez J, Honorato CG, Pérez, MA, Toscano JJ. $\gamma\gamma \to \phi_i\phi_j$ processes in the type-III two-Higgs-doublet model. Physical Review D 2012; 85: 015020. doi: 10.1103/PhysRevD.85.015020

[19] Branco GC, Ferreira PM, Lavoura L, Rebelo MN, Sher M et al. Theory and phenomenology of two-Higgs-doublet models. Physics Reports 2012; 516: 1-102. doi: 10.1016/j.physrep.2012.02.002

[20] Glashow SL, Weinberg S. Natural conservation laws for neutral currents. Physical Review D 1977; 15: 1958. doi: 10.1103/PhysRevD.15.1958

[21] Gunion JF, Haber HE. CP-conserving two-Higgs-doublet model: the approach to the decoupling limit. Physical Review D 2003; 67: 075019. doi: 10.1103/PhysRevD.67.075019

[22] Carena M, Low I, Shah NR, Wagner CEM. Impersonating the Standard Model Higgs boson: alignment without decoupling. Journal of High Energy Physics 2014; 2014; 15. doi: 10.1007/JHEP04(2014)015

[23] Deshpande NG, Ma E. Pattern of symmetry breaking with two Higgs doublets. Physical Review D 1978; 18: 2574. doi: 10.1103/PhysRevD.18.2574

[24] Sher M. Electroweak Higgs potentials and vacuum stability. Physics Reports 1989; 179: 273-418. doi: 10.1016/0370-1573(89)90061-6

[25] Ferreira PM, Santos R, Barroso A. Stability of the tree-level vacuum in two Higgs doublet models against charge or CP spontaneous violation. Physics Letters B 2004; 603: 219-229. doi: 10.1016/j.physletb.2004.10.022.

[26] Kanemura S, Yagyu K. Unitarity bound in the most general two Higgs doublet model. Physics Letters B 2015; 751: 289-296. doi: 10.1016/j.physletb.2015.10.047

[27] Akeroyd AG, Arhrib A, Naimi EM. Note on tree-level unitarity in the general two Higgs doublet model. Physics Letters B 2000; 490: 119-124. doi: 10.1016/S0370-2693(00)00962-X

[28] Horejsi J, Kladiva M. Tree-unitarity bounds for THDM Higgs masses revisited. European Physical Journal C 2006; 46: 81-91. doi: 10.1140/epjc/s2006-02472-3

[29] Ginzburg IF, Ivanov IP. Tree-level unitarity constraints in the most general 2HDM. Physical Review D 2005; 72: 115010. doi: 10.1103/PhysRevD.72.115010

[30] Aaboud M, Aad G, Abbott B, Abdinov O, Abeloos B et al. Search for a heavy Higgs boson decaying into a Z boson and another heavy Higgs boson in the *llbb* final state in pp collisions at $\sqrt{s} = 13$ TeV with the ATLAS detector. Physics Letters B 2018; 783: 392. doi: 10.1016/j.physletb.2018.07.006

[31] Aad G, Abbott B, Abdallah J, Khalek SA, Abdinov O et al. Search for a CP-odd Higgs boson decaying to Zh in pp collisions at $\sqrt{s} = 8$ TeV with the ATLAS detector. Physics Letters B 2015; 744: 163. doi: 10.1016/j.physletb.2015.03.054

[32] Aad G, Abbott B, Abdallah J, Abdinov O, Aben R et al. Search for an additional, heavy Higgs boson in the $H \to ZZ$ decay channel at $\sqrt{s} = 8$ TeV in pp collision data with the ATLAS detector. The European Physical Journal C 2016; 76: 45. doi: 10.1140/epjc/s10052-015-3820-z

[33] Misiak M, Asatrian HM, Boughezal R, Czakon M, Ewerth T et al. Updated NNLO QCD predictions for the weak radiative B-meson decays. Physical Review Letters 2015; 114: 221801. doi: 10.1103/PhysRevLett.114.221801

[34] Misiak M, Steinhauser M. Weak radiative decays of the B meson and bounds on $M_{H^\pm}$ in the two-Higgs-doublet model. European Physical Journal C 2017; 77: 201. doi: 10.1140/epjc/s10052-017-4776-y

[35] Enomoto T, Watanabe R. Flavor constraints on the two Higgs doublet models of Z_2 symmetric and aligned types. Journal of High Energy Physics 2016; 1605: 2. doi: 10.1007/JHEP05(2016)002

[36] Arhrib A, Benbrik R, Moretti S. Bosonic decays of charged Higgs bosons in a 2HDM type-I. European Physical Journal C 2017; 77; 621. doi: 10.1140/epjc/s10052-017-5197-7

[37] Aad G, Abbott B, Abdallah J, Khalek SA, Abdinov O et al. Search for charged Higgs bosons decaying via $H^\pm \to \tau^\pm \nu$ in fully hadronic final states using *pp* collision data at $\sqrt{s} = 8$ TeV with the ATLAS detector. Journal of High Energy Physics 2015; 1503: 88. doi: 10.1007/JHEP03(2015)088

[38] Khachatryan V, Sirunyan AM, Tumasyan A, Adam W, Asilar E et al. Search for a charged Higgs boson in pp collisions at $\sqrt{s} = 8$ TeV. Journal of High Energy Physics 2015; 1511: 018. doi: 10.1007/JHEP11(2015)018

[39] Khachatryan V, Sirunyan AM, Tumasyan A, Adam W, Asilar E et al. Search for a light charged Higgs boson decaying to $c\bar{s}$ in pp collisions at $\sqrt{s} = 8$ TeV. Journal of High Energy Physics 2015; 1512: 178. doi: 10.1007/JHEP12(2015)178

[40] Aad G, Abajyan T, Abbott B, Abdallah J, Khalek SA et al. Search for a light charged Higgs boson in the decay channel $H^+ \to c\bar{s}$ in $t\bar{t}$ events using pp collisions at $\sqrt{s} = 7$ TeV with the ATLAS detector. European Physical Journal C 2013; 73: 2465. doi: 10.1140/epjc/s10052-013-2465-z

[41] ALEPH, DELPHI, L3, OPAL, LEP Collaborations. Search for charged Higgs bosons: combined results using LEP data. European Physical Journal C 2013; 73: 2463. doi: 10.1140/epjc/s10052-013-2463-1

[42] Akeroyd AG, Aoki M, Arhrib A, Basso L, Ginzburg IF et al. Prospects for charged Higgs searches at the LHC. European Physical Journal C 2017; 77: 276. doi: 10.1140/epjc/s10052-017-4829-2

[43] Moretti S. 2HDM charged Higgs boson searches at the LHC: status and prospects. In: 6th International Workshop on Prospects for Charged Higgs Discovery at Colliders; Uppsala, Sweden; 2016.

[44] Tanabashi M, Hagiwara K, Hikasa K, Nakamura K, Sumino Y et al. Review of particle physics. Physical Review D 2018; 98: 03001. doi: 10.1103/PhysRevD.98.030001

[45] Eriksson D, Rathsman J, Stal O. 2HDMC - two-Higgs-doublet model calculator. Computer Physics Communications 2010; 181: 189-205. doi: 10.1016/j.cpc.2009.09.011

[46] Eriksson D, Rathsman J, Stal O. HDMC — two-Higgs-doublet model calculator. Computer Physics Communications 2010; 181: 833-834. doi: 10.1016/j.cpc.2009.12.016

[47] Bechtle P, Brein O, Heinemeyer S, Weiglein G, Williams KE. HiggsBounds: Confronting arbitrary Higgs sectors with exclusion bounds from LEP and the Tevatron. Computer Physics Communications 2010; 181: 138-167. doi: 10.1016/j.cpc.2009.09.003

[48] Bechtle P, Heinemeyer S, Stål O, Stefaniak T, Weiglein G. HiggsSignals: Confronting arbitrary Higgs sectors with measurements at the Tevatron and the LHC. European Physical Journal C 2014; 74: 2711. doi: 10.1140/epjc/s10052-013-2711-4

[49] Binosi D, Theussl L. JaxoDraw: A graphical user interface for drawing Feynman diagrams. Computer Physics Communications 2004; 161: 76-86. doi: 10.1016/j.cpc.2004.05.001

[50] Küblbeck J, Böhm M, Denner A. Feynarts - computer-algebraic generation of Feynman graphs and amplitudes. Computer Physics Communications 1990; 60: 165-180. doi: 10.1016/0010-4655(90)90001-H

[51] Hahn T. Generating Feynman diagrams and amplitudes with FeynArts3. Computer Physics Communications 2001; 140: 418-431. doi: 10.1016/S0010-4655(01)00290-9

[52] Hooft G, Veltman M. Regularization and renormalization of gauge fields. Nuclear Physics B 1972; 44: 189-213. doi: 10.1016/0550-3213(72)90279-9

[53] Passarino G, Veltman, M. One-loop corrections for e^+e^- annihilation into $\mu^+\mu^-$ in the Weinberg model. Nuclear Physics B 1979; 160: 151-207. doi: 10.1016/0550-3213(79)90234-7

[54] Telnov VI. Problems in obtaining $\gamma\gamma$ and γe colliding beams at linear colliders. Nuclear Instruments and Methods in Physics Research A 1990; 294: 72-92. doi: 10.1016/0168-9002(90)91826-W

[55] Hahn T, Schappacher C. The implementation of the Minimal Supersymmetric Standard Model in FeynArts and FormCalc. Computer Physics Communications 2002; 143: 54. doi: 10.1016/S0010-4655(01)00436-2

[56] Hahn T, Perez-Victoria M. Automated one-loop calculations in four and D dimensions. Computer Physics Communications 1999; 118: 153-165. doi: 10.1016/S0010-4655(98)00173-8

[57] Zarnecki AF. CompAZ: parametrization of the luminosity spectra for the photon collider. Acta Physica Polonica B 2003; 34: 2741.

[58] Demirci M, Ahmadov AI. Neutralino pair production via photon-photon collisions at the ILC. Physical Review D 2016; 94: 075025. doi: 10.1103/PhysRevD.94.075025

[59] Demirci M. Associated production of Higgs boson with a photon at electron-positron colliders. arXiv: 1905.09363 [hep-ph].